Journal of Catalysis 454 (2026) 116658

Contents lists available at ScienceDirect

Journal of Catalysis

journal homepage: www.elsevier.com/locate/jcat

Research article

Protonation dynamics of confined ethanol–water mixtures in H-ZSM-5 from machine learning-driven metadynamics☆

Princy Jarngal [a], Benjamin A. Jackson [b], Simuck F. Yuk [c], Difan Zhang [d], Mal-Soon Lee [b], Maria Cristina Menziani [e], Vassiliki-Alexandra Glezakou [d,*], Roger Rousseau [d], GiovanniMaria Piccini [e,*]

[a] Multiscale Modeling of Heterogeneous Catalysis in Energy Systems, The Fuel Science Center, RWTH Aachen University, Schinkelstraße 8, Aachen 52062, Germany
[b] Institute for Integrated Catalysis, Pacific Northwest National Laboratory, Richland, WA 99352, USA
[c] Department of Chemical and Biological Science and Engineering, United States Military Academy, West Point, New York 10996, USA
[d] Chemical Sciences Division, Oak Ridge National Laboratory, Oak Ridge, TN 37831, USA
[e] Department of Chemical and Geological Sciences, University of Modena and Reggio Emilia, Via G. Campi 103, 41125 Modena, Italy

ARTICLE INFO

Keywords:
Protonation equilibrium
Molecular dynamics
Metadynamics
Machine learning
Global optimization

ABSTRACT

Zeolites are indispensable heterogeneous catalysts in industrial chemical processes, valued for their strong Brønsted acidity, well-defined microporous frameworks, and tunable pore structures. Their catalytic activity arises primarily from Brønsted acid sites (BAS), typically present as bridging hydroxyl groups (Si–OH–Al). Under aqueous reaction conditions, these protons interact dynamically with water and alcohol molecules, leading to complex solvation and protonation behavior within confined pores. In this study, we investigate the protonation equilibrium occurring between ethanol and water at the BAS of acidic zeolites under varying hydration levels, i.e., $C_2H_5OH–(H_2O)_n$, n = 1–4. Local structure was analyzed through an adaptive-learning global optimization algorithm, while enhanced sampling molecular dynamics simulations with Well-Tempered Metadynamics (WTMetaD) and machine learning interatomic potentials (MLPs) provide free-energy surfaces (FES) at variable hydration levels. The results reveal a strong dependence of proton localization on the degree of hydration. In presence of just 1 water molecule, the proton resides predominantly on ethanol; with 2 water molecules, it shifts toward water, and starting at 3, it becomes delocalized over the water cluster. These findings underscore the critical role of solvation in modulating acid site behavior and suggest that a minimum of three water molecules is necessary to fully stabilize the proton on water within the zeolite framework. This solvation threshold has significant implications for catalytic processes, particularly in biomass conversion reactions where alcohol protonation is a key step in dehydration mechanisms.

1. Introduction

Zeolites are crystalline microporous aluminosilicates comprising a three-dimensional framework of corner-sharing SiO_4 tetrahedra. Upon substitution of silicon by trivalent atoms, most commonly aluminum, introduces a net negative charge in the lattice which is typically balanced by extra framework cations. When this charge is compensated by protons, Brønsted acid sites (BAS) comprising —Si–(OH)–Al moieties are formed. These protonic sites serve as the primary centers for proton donation and are responsible for the strong acidity of zeolites [1]. In addition to their exceptional catalytic activity, zeolites offer advantages like well-defined confinement effects, high thermal stability, shape-selectivity, and tunable adsorption. Owing to these properties, zeolites are extensively used as solid acid catalysts in processes such as hydrocarbon cracking, alcohol dehydration, isomerization, alkylation, aldol condensation and esterification [2–12].

More recently attracted growing attention for the catalytic conversion of biomass-derived alcohols which represent renewable and carbon–neutral alternatives to fossil feedstocks [13–17]. Fermentation of lignocellulose biomass yield complex aqueous mixtures of linear, cyclic, and aromatic alcohols [13,15]. In such water-rich environments, the nature of BAS is significantly altered due to solvation of BAS by water

☆ This article is part of a special issue entitled: 'Molecular Dynamics in Catalysis' published in Journal of Catalysis.

* Corresponding authors.
E-mail addresses: glezakouva@ornl.gov (V.-A. Glezakou), giovannimaria.piccini@unimore.it (G. Piccini).

https://doi.org/10.1016/j.jcat.2025.116658
Received 6 October 2025; Received in revised form 26 November 2025; Accepted 22 December 2025
Available online 23 December 2025

leading to the formation of protonic species, hydronium ions ($H_3O^+(H_2O)_n$), confined within the zeolite nanopores. This transformation has been characterized by various techniques such as extended X-ray absorption fine structure, ^{27}Al magic-angle spinning nuclear magnetic resonance (NMR) spectroscopy and vibrational spectroscopic studies [18–26]. The confined water solvation microenvironment in zeolites not only changes the nature of catalytically active site but also strongly affects the reactivity and selectivity [27–29]. Analogous effects have been observed in self-assembled supramolecular systems [30–35]. Consequently understanding the solvation structure of water and its role in proton transfer at BAS has attracted intense research interest over the past two decades, with numerous experimental and theoretical studies focusing on the question: How many water molecules are needed to drive the transfer of proton from BAS to adsorbed water molecules [27,36]?

At low hydration levels (i.e., one water molecule per BAS), both quantum mechanical (QM) calculations [37,38] including Hartree–Fock (HF), Møller–Plesset perturbation theory of second order (MP2) [39], and density functional theory (DFT) as well as spectroscopic investigations [20,26,40,41] have consistently shown that water forms a hydrogen-bonded complex with the BAS rather than undergoing full proton transfer [25,37]. The presence of this neutral adduct is strongly supported by experimental vibrational signatures, particularly the infrared (IR) bands observed at ~2800 and 2400 cm^{-1} [26,37,38] and further corroborated by inelastic neutron scattering (INS) studies [41]. Similar adsorption behaviors are observed in anhydrous single [42] or double alcohol adsorption [43] at the BAS. Further computational studies showed the neutral complex as a local minimum on the potential energy surface under these low hydration conditions [21,37,38].

As the hydration level increases to two water molecules per BAS, the picture becomes more ambiguous. A combined powder neutron diffraction and infrared spectroscopy study suggested the coexistence of both neutral and protonated water complexes [20]. Earlier static DFT calculations [37,38] and *ab initio* quantum chemical simulations [44] proposed that water dimers may possess sufficient proton affinity to form protonated ion-pair complexes. However, subsequent Car-Parrinello molecular dynamics challenged this notion, suggesting that a minimum of three water molecules is required to stabilize $H_3O^+(H_2O)_2$, as the first thermodynamically stable protonated cluster [21]. These studies also reflect that both the neutral water dimer and the ion pair structure are energetically competitive, but the relative stability of protonated water dimer was highly sensitive to the functional choice and simulation conditions [38,45–51]. Nonetheless, finite-temperature molecular dynamics (MD) simulations [47,50,52], along with enhanced sampling MD [49], have demonstrated increase in proton affinity of water cluster with the number of water molecules [53–55], highlighting the thermodynamic favorability of larger hydrated proton clusters.

Recent spectroscopic studies, including high-resolution NMR and 2D-IR provide compelling evidence for proton transfer at elevated hydration levels. For water loadings between 2 and 9 molecules per BAS, Lercher and co-workers identified a signature ^1H NMR resonance at 9 ppm, consistent with the presence of hydrated hydronium ions [56]. This observation aligns with an earlier theoretical predictions, which reported a chemical shift of 9.5 ppm shift for protonated water dimers [57]. Metadynamics simulations [58,59] using Voronoi tessellation-based collective variables (CV) [49,60,61] across various zeolite frameworks have further illuminated the that at low hydration ($\leq 2H_2O$ per BAS) the proton remains shared between the BAS and a water molecule, whereas at higher hydration (3–8H_2O per BAS) it becomes fully solvated within water clusters. This transition demonstrates a shift in the nature of the acid site in zeolites from a localized, framework bound proton donor site to a dynamic, delocalized proton reservoir. Such confined hydronium ions exhibit markedly different catalytic behavior compared to traditional aqueous acid solutions [62,63]. For instance, the hydrated hydronium ions in the zeolite pores enhance cyclohexanol dehydration rates by two orders of magnitude compared to the rates in aqueous solution due to enthalpic and entropic stabilization of reactive intermediates [64–67]. Similarly, confinement-induced structural reorganization of water, particularly into 3D-hydrogen-bonded clusters in larger cages and 1D-oligomeric chains in narrower channel [68,69] can increase turnover rates by as much as 400-fold in reactions such as alkene epoxidation due to significant entropic gains [70]. Comparable enhancements are observed in the O-demethylation of guaiacol, where under-coordinated hydronium ions confined within zeolite boost reaction rates. These solvation confinement effects extend beyond oxygenates, in hydrocarbon transformations like cumene dealkylation [71] water has been shown to increase reactivity by entropically stabilizing transition state despite elevating activation enthalpies. Other studies have shown that alcohol–water–proton clusters form extended hydrogen-bonded networks which directly impacts transition state stabilization and catalytic rates [72–74]. Nevertheless, the influence of hydration on catalysis within zeolites is nuanced and not uniformly advantageous. In certain cases, water can inhibit catalytic activity. The dehydration of 1-propanol proceeds more slowly in hydrated environments due to preferential stabilization of the reactant relative to the transition state [75,76]. Similar trend is observed in alkane C–H bond activation, where higher water loadings (>2–3 H_2O) diminish reaction rates [77]. The formation of such hydrated ionic species within confined micropores can also limit substrate adsorption due to steric constraints, ultimately diminishing overall turnover rates. In parallel, polar aprotic solvents have demonstrated the ability to modulate proton availability, enhancing catalytic performance by selectively stabilizing protonated intermediates over high-energy transition states particularly in biomass conversion processes [78,79].

Overall, when aqueous solution of biomass-derived alcohols come in contact with BAS under confined environments, a complex network of solvation effects emerges. The interplay of acid strength, hydration level, type of substrate, and confinement within the microporous framework led to nontrivial protonation equilibria and reaction pathways [80]. This complexity raises a fundamental question that remains largely unexplored: How does the thermodynamics of protonation by the BAS evolve with increasing hydration in the presence of C_{2+} organic alcohols?

Addressing this question requires a molecular-level understanding of solvation dynamics and proton delocalization. The evolution of the catalytic active site from a static BAS proton source to a dynamic, reactive interface, challenges conventional *ab initio* static models which fail in capturing the highly intricate solvation dynamics of the delocalized proton. *Ab initio* molecular dynamics (AIMD) provides a valuable tool to address this challenge by accounting for thermal motion and explicit solvent interactions at the atomic level. However, AIMD suffers from inherent timescale limitations, which hinder its ability to capture rare events such as proton transfer or slow equilibrium transitions that are essential for understanding catalytic mechanisms.

To overcome these limitations, enhanced sampling methods such as Well-Tempered Metadynamics (WTMetaD) [59] are effective to accelerate sampling across high free energy barriers and explore the relevant configurational space. Despite their utility, these simulations remain computationally demanding when used in combination with QM force evaluation. To alleviate the computational burden while retaining QM accuracy, we adopt graph neural network (GNN) [81] based machine learning potentials (MLPs) as a powerful surrogate [82–85]. By learning the underlying potential energy surface from high quality reference data obtained from DFT-based enhanced sampling in zeolites at finite temperature, MLPs enable large-scale simulations ensuring exhaustive sampling. The key advantage of this approach lies in the substantial computational acceleration it offers.

Using this approach, we carried out enhanced sampling WTMetaD simulations to investigate the protonation equilibrium of ethanol in H-ZSM-5 in the presence of varying water content. Free energy surfaces (FES) reveal a strong dependence of proton location on water loading: At

1 water molecule adsorption (C_2H_5OH–H_2O), the protonation equilibrium is shifted towards alcohol, at two water molecules (C_2H_5OH–$(H_2O)_2$), the proton is likely to sit between ethanol and water, whereas at 3 content (C_2H_5OH–$(H_2O)_3$) it starts resembling more the bulk solution conditions, the proton is delocalized in the water cluster with a much lower probability of sitting on the ethanol OH group. This behavior underscores the central role of the micro-hydration environment in dictating proton transfer thermodynamics and thus modulating catalytic activity. Such detailed understanding of water–substrate–acid site interactions is essential for elucidating reaction mechanisms and guiding the rational design of zeolite-based catalysts for sustainable biomass conversion.

2. Methods

2.1. PES exploration via RANGE

A potential energy surface (PES) exploration was performed using RANGE [86] to identify the most favorable interaction configurations of one ethanol molecule with one, two, or three water molecules in the H-ZSM-5 zeolite pore near the BAS. For each case, the pore space near the BAS site was first identified, and an ethanol molecule, along with one, two, or three water molecules, was placed in the BAS region. RANGE then guided the placement of the molecules and systematically searched for low-energy configurations that a standard optimization process could have missed. The Universal Force Field (UFF) [87] was used with RANGE for a preliminary geometry optimization, followed by a full geometry optimization using the MACE force field (the pretrained MACE-MPA-0 foundation model) [88] for on-the-fly optimization with RANGE. The MACE force field was chosen because of its accuracy against DFT calculated energies and atomic forces that demonstrated the fidelity of the force field. (see Fig. S5 of Supplementary Information (SI) for additional details).

For each system (one ethanol molecule with one, two, or three water molecules, respectively), a minimum of 20,000 structures were explored, and the resulting structures were ranked by their energies. The 1,000 lowest-energy configurations were further grouped by their structural similarities to the ground-state configuration (the lowest energy) using the positions of C, H, O, and Al atoms in the BAS, ethanol, and water. The cosine similarity [89,90] was used with a threshold of 0.1 to define a group. Configurations in the same group have closer similarities and indicate similar adsorptive configurations. Representative structures from each group then demonstrate different adsorption configurations of ethanol and water molecules at the BAS. These representative structures were further re-optimized by DFT (same settings as in Section 2.2) to obtain refined geometries and energies at the DFT level. They were also compared with the annealed AIMD structures, see Section 2 of SI, to show the larger variety of adsorptive configurations beyond the sampled structures by AIMD thermal annealing simulations. This comparison allows for an evaluation of alternative methods of low-computational cost, such as a global optimization procedure, to explore the potential energy surface and generate a good initial configuration before starting more costly AIMD, which can factor in both energy and entropy. We note that one could still use a Boltzmann weighing factor or simple harmonic corrections on top of the energies of individual configurations to recover thermal approximations to free energy, however the reliability of this approximation will largely depend on the degree of anharmonicity of the system [91].

2.2. MLP-driven WTMetaD simulations

To accurately capture the dynamics of proton transfer among the BAS, ethanol and water, including thermal effects such as entropy and anharmonicity, WTMetaD simulations were performed. As with all metadynamics simulations, defining suitable CVs is essential for effectively enhancing sampling of rare events such as proton transfer [58,92]. Two in-house designed CVs [49,60,61] previously demonstrated to be highly versatile for proton transfer reactions, were used to describe proton transfer dynamics between BAS, ethanol, and water as well as diffusion of protonated species inside the zeolite cavities.

The first CV, S_p, identifies the location of the excess proton. Voronoi tessellation based on the oxygens atoms of BAS, ethanol, and water partitions the system into polyhedra centered on protonation sites which represent the spatial region closest to the given protonation site [60]. Hydrogen atoms are initially assigned to these sites in their neutral configurations: one to the BAS (defined by the four acidic oxygens adjacent to Al), one to ethanol, and two to water. S_p, thus serves as a protonation state variable that distinguishes between protonated ethanol, water, and BAS species. Specifically, S_p approaches 0 when the excess proton resides on the BAS within the zeolite framework, 1 when ethanol is protonated, and 3 when protonated water dominates. (see CV1 in Section 4.1.1 of the SI for detailed explanation). The second CV, S_d, derived via Harmonic Linear Discriminant Analysis (HLDA) [93,94] determines the overall distance between the proton donating and accepting site, typically the BAS and the protonated ethanol or water molecules. This CV enhances sampling of proton diffusion by tracking spatial delocalization of the protonated entities within the zeolite pores (see CV2 in Section 4.1.2 of SI). Together, these CVs provide a clear and continuous description of proton transfer and diffusion within the confined ethanol–water mixtures in zeolites.

To generate a reliable MLP using MACE [81] suitable for running long-timescale WTMetaD simulations, we initiated our workflow with short *ab initio* WTMetaD simulations across a series of ethanol–water mixtures, C_2H_5OH–$(H_2O)_n$, $n = 1$– 3 (~60 ps each) after proper equilibration. Details of the system setup and equilibration are provided in Section 1 of the SI. These initial DFT-WTMetaD simulations were carried out with the Perdew-Burke-Ernzerhof (PBE) [95] exchange–correlation functional within the generalized gradient approximation (GGA) using with Grimme's semiempirical D3 dispersion [96] correction. To ensure computational efficiency during the initial exploratory metadynamics simulations, we employed the DZVP-MOLOPT basis set [97], the corresponding Goedecker–Teter–Hutter (GTH) pseudopotential [98–100], a plane wave cutoff of 280 Ry and a standard SCF convergence thresholds of 10^{-6} Hartree. The primary objective at this stage was to sample diverse regions of the proton transfer free energy landscape rather than to achieve highly accurate energy/force estimates. All configurations selected for training the MLP were subsequently re-evaluated at higher accuracy, using PBE + D3 with the TZVP-MOLOPT basis set, a higher plane-wave cutoff tighter SCF convergence threshold, as described below. All DFT calculations were performed using the CP2K code [101] patched with PLUMED [102], an open source plugin for enhanced sampling. The initial set of *ab initio* enhanced sampling simulations sampled multiple proton transfer events between the BAS and surrounding ethanol or water molecules, effectively exploring the relevant regions of the free energy surface and generating chemically meaningful configurations for training the MLP.

Crucially, the fidelity of MLPs depends on a training dataset that sufficiently captures the chemical and conformational diversity of the system, especially in solution-phase environments characterized by flexible solvent networks and dynamic proton transfer events. To ensure diversity and avoid redundancy in the training dataset, we employed a descriptor-based selection strategy using the Smooth Overlap of Atomic Positions (SOAP) descriptor [103] for screening DFT trajectories. SOAP encodes both geometric and chemical features of local atomic environments in a rotationally and translationally invariant manner making it ideal for identifying unique configurations. Taking inspiration from the work of Zhang *et al.* [104] we quantified structural similarity between configurations based on their SOAP kernel values. A new configuration was included only if its maximum kernel similarity to existing entries in the training set was below a predefined threshold. This approach yielded an initial dataset of 1906 configurations. SOAP descriptors were computed using the DScribe library [105] with a 6 Å radial cutoff, and

expansion parameters $n_{max} = 12$ and $l_{max} = 8$, focused on the environments surrounding the BAS, ethanol, and water molecules.

The final reference energy and force labels for the selected configurations were calculated using the PBE + D3 [95] dispersion correction [106,107] and TZVP-MOLOPT basis set with a plane-wave cutoff of 800 Ry and SCF convergence threshold of 10^{-8} Hatree. These high-fidelity data points formed the foundation for training the initial MLP (see Section 3 of the SI for training details).

To systematically improve the MLP and enrich the training dataset, we implemented an active learning framework. The initial MLP was used to perform exploratory MLP-driven WTMetaD simulations across different ethanol–water mixtures. Configurations showing poor prediction confidence were selectively identified using a Query-by-Committee (QBC) criteria [108]. This involved training an ensemble of MACE models and quantifying uncertainty based on the maximum standard deviation in predicted atomic forces across the ensemble. SOAP similarity matrices-based screening was applied to filter out configurations with high structural overlap relative to existing training data. These newly selected set of high-uncertainty configurations were recomputed with DFT to obtain accurate energy and force labels for MLP retraining. After two iterations of the active learning loop, the dataset expanded to 3076 structures, spanning a broad chemical space.

The final MLP achieved force RMSE of 11.9 meV/Å and energy per atom RMSE of 0.3 meV on the validation set and demonstrated excellent stability in long-timescale simulations. This trained MLP was subsequently used to perform WTMetaD simulations under the canonical (NVT) ensemble at 300 K, extending sampling to longer timescales (up to ~4 ns) and broader configurational spaces for systems containing 1–4 water molecules per ethanol molecule. Results for the system with four water molecules are presented in Section 4.2 of the SI. Additional simulations on pure ethanol and pure water were also performed to establish baselines for evaluating protonation equilibria in the absence of co-solvents. All MLP-driven WTMetaD simulations were performed in LAMMPS [109] patched with PLUMED [102].

This integrated approach combining global optimization with MLP-accelerated enhanced sampling enables the exploration of protonation phenomena with unprecedented accuracy and efficiency. It provides valuable mechanistic insights into the behavior of acid zeolites in aqueous environments, while simultaneously validating a hierarchical computational protocol for complex reactive systems.

3. Results

3.1. PES exploration using RANGE

The PES exploration using RANGE is illustrated in Fig. 1. For all three systems with one, two, or three water molecules, RANGE effectively sampled a wide variety of structures across a broad energy range. By analyzing the 1,000 lowest-energy configurations in each case, we identified several representative structures from the MACE scan of PES, followed by DFT refinement. Below, we discuss the minima found within ~10 kJ/mol from the ground state for each system.

For the 1 H_2O case (red in Fig. 1), the global minimum corresponds to a protonated ethanol molecule in a Zundel-like configuration with the H_2O closing a ring with two hydrogen bonds with the BAS. Further, we identify the closest local minimum where only the protonated ethanol interacts with the BAS through only one hydrogen bond, with an energy of +8.6 kJ/mol. Another local minimum (at +10.1 kJ/mol) involves a protonated water directly bound to the BAS. Overall, the protonated ethanol is favored over the protonated water, consistent with their gas-

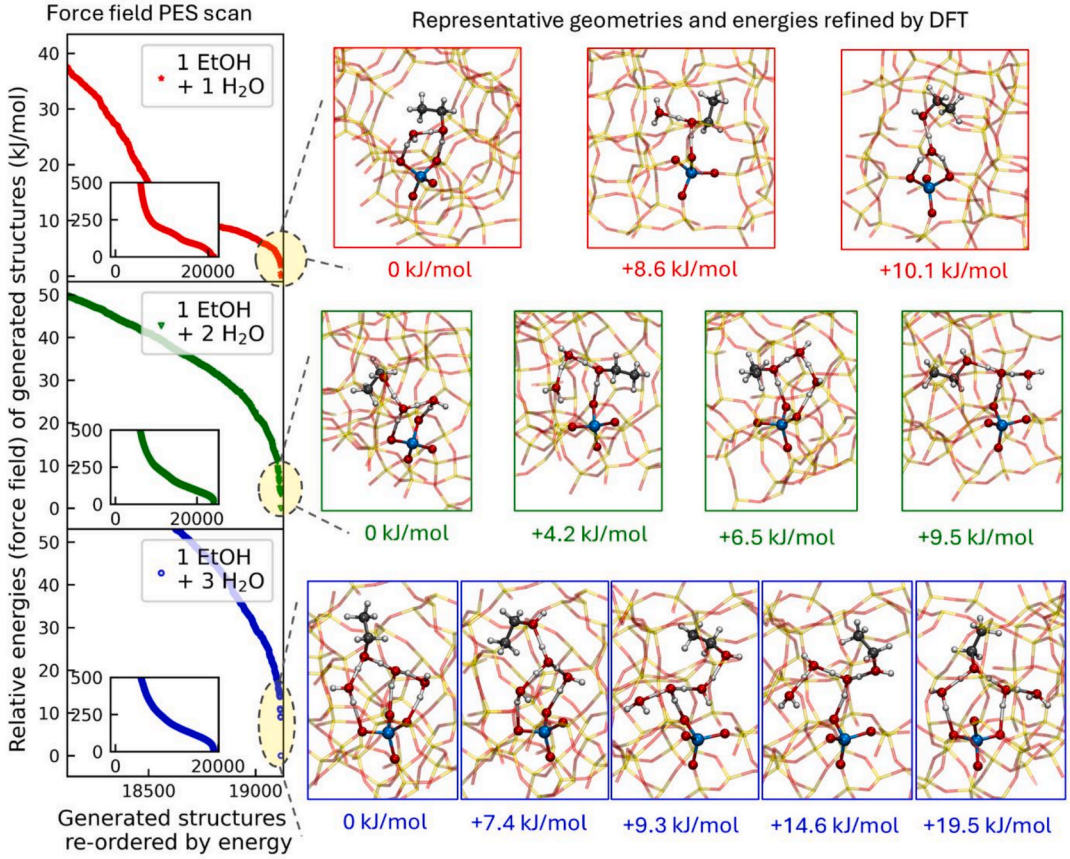

Fig. 1. Structural search for the most favorable binding configurations of one ethanol molecule with one, two, or three water molecules in the pore space near the BAS site of H-ZSM-5 zeolite. The left column shows the energy profiles of the 1,000 lowest-energy structures, with the inset displaying the full energy landscape. The right column presents representative structures further refined by DFT and their relative DFT energies with respect to the global minimum.

phase basicity. Given that the 20,000 structures of a system of approximately 300 atoms were sampled in a matter of hours, these results suggest that RANGE is an effective tool for configurational sampling of large model systems and identifies low-energy adsorptive configurations without prior assumptions.

For the 2 H_2O case (green in Fig. 1), the global minimum finds two water molecules bound to the BAS (Zundel), with the ethanol hydrogen-bound to the protonated water. A local minimum at only +4.2 kJ/mol arises when only the protonated ethanol directly binds to the BAS, with the proton shared between ethanol and one water molecule, and the second water molecule is hydrogen-bound to the first water. Another higher local minimum at +6.5 kJ/mol occurs with a protonated water bound to both ethanol and the other water, and all hydrogen-bound to the BAS. Finally, a third local minimum at +9.5 kJ/mol is found with 1 hydrogen bond to the BAS, the other water and the ethanol. Overall, at this hydration level, ethanol and water compete for the BAS H, which underscores the importance of the reaction environment in determining the relative basicity of the sites.

In the 3 H_2O case (blue in Fig. 1), the global minimum corresponds to all three water molecules bound to the BAS and the ethanol, which bridges a protonated water and another water molecule. The closest local minimum (at +7.4 kJ/mol) involves an Eigen-like H_3O^+ hydrogen-bound to two waters and the ethanol molecule. Two other local minima (+9.3 kJ/mol and +14.6 kJ/mol) involve only the protonated water bound to the BAS, with ethanol binding to either another water or the protonated water. A higher-energy local minimum (+19.5 kJ/mol) involves a protonated ethanol bound to two water molecules that are bound to the BAS. In summary, these structures indicate a stronger preference for protonated water over protonated ethanol.

Overall, the global optimization with RANGE demonstrates a robust exploration of the complex PES for ethanol adsorbed near the BAS of H-ZSM-5 pores at different hydration states. The lower-lying configurations demonstrate a shift of the preferred protonation state from ethanol to water as the number of water molecules increases from one to three. In addition, compared to the adsorption configurations obtained from AIMD thermal annealing simulations (see Fig. S1 in Section 2 of the SI), the RANGE search identifies a broader set of low-energy configurations that are not readily captured by the AIMD annealing approach. Notably, the computational cost of the RANGE search is less than 10 % of that of the AIMD annealing simulations, highlighting the efficiency of the

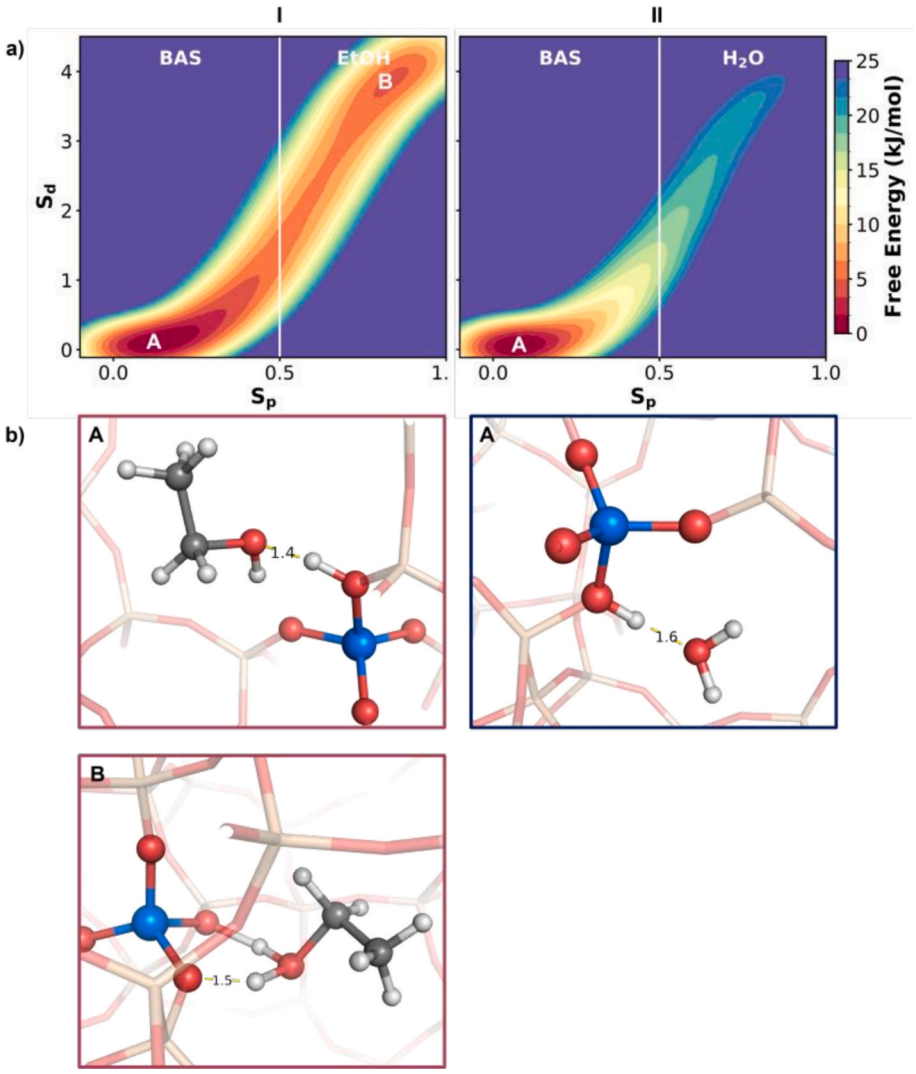

Fig. 2. a) Free energy surfaces representing the protonation equilibrium of ethanol and water by BAS proton computed via statistical reweighting of enhanced sampling simulations. The surfaces are plotted along two collective variables: S_p, which describes the position of the excess proton, and, representing S_d the distance between the proton carrier and the BAS. b) Representative structures from a collection of snapshots extracted by FESTA for each free energy basin. Labeled hydrogen bond lengths are in Å. Atom color coding: aluminum (blue), oxygen (red), hydrogen (white), carbon (grey). For clarity, the silicon and oxygen atoms of the zeolite framework are shown in a transparent representation. (For interpretation of the references to colour in this figure legend, the reader is referred to the web version of this article.)

approach to quickly assess a PES. However, this search by RANGE does not consider temperature effects, and it is purely enthalpy-driven, neglecting entropic effects.

3.2. WTMetaD simulations

3.2.1. Protonation of ethanol and water: baseline cases

To better understand the distinct protonation behavior of ethanol and water, we first calculated their protonation thermodynamics when interacting individually with the BAS. Using our trained MLP, we carried out WTMetaD simulations of the isolated protonation of ethanol and water by the BAS proton. The simulations employed CVs that capture both the protonation state of the adsorbed species at the BAS and the distance between the proton carrier and the BAS site. In this setup, only two configurations are possible: proton shared between BAS and water, or between BAS and ethanol. Accordingly, S_p is defined that $S_p = 0$ corresponds to the proton located at the BAS, and $S_p = 1$ corresponds to complete protolysis of ethanol or water, as shown in the FES for both cases (Fig. 2a).

Our results for the single water adsorption case are consistent with the previous computational and experimental studies, which have shown that a neutral adsorption complex at the BAS is the thermodynamically favored species, rather than a protonated water (H_3O^+) [56,110]. The proton from the BAS is not sufficiently stabilized by a single water molecule; thus, proton transfer does not occur. This is supported by the absence of a minimum corresponding to protonated water in FES. These findings reinforce the established understanding of the protonation state of BAS and an adsorbed water molecule under low hydration conditions.

In contrast, the case of a single ethanol at the BAS reveals distinct structural characteristics. The FES indicates that protonated ethanol is energetically more favorable than protonated water, with a notable energy difference (Fig. 3), similar to the results obtained by RANGE. Additionally, the energy barrier for ethanol protonation is substantially lower (~5 kJ/mol) than for water. This suggests that, under single-molecule adsorption conditions, ethanol's structural properties such as its ability to better accommodate the proton and stabilize the resulting cation outweigh the proton affinity of water clusters due to polarization. This can also be inferred from the slight difference in the average hydrogen-bond distances between ethanol (or water) and BAS proton in minima A of the FES surfaces shown in Fig. 2a. The structures corresponding to the minima A characterized by $S_p = 0$, $S_d = 0$ were in both the system with only water and only ethanol were extracted with our recently developed code FESTA (Free Energy Surface Trajectory Analysis) [111]. It is an automated tool that efficiently identifies relevant free energy minima using a connected-component labeling algorithm and extracts representative trajectory frames via a Shapely-polygon-based analysis. This approach enables the systematic extraction of structures corresponding to FES minimum from enhanced sampling simulations. The hydrogen bond between ethanol oxygen and the BAS proton is shorter (1.47 Å) than that between water oxygen and the BAS proton (1.64 Å). This mechanistic distinction is crucial for understanding the initial steps of catalytic reactions in zeolites and explain the observed differences in protonation behavior between water and alcohol under low-coverage conditions.

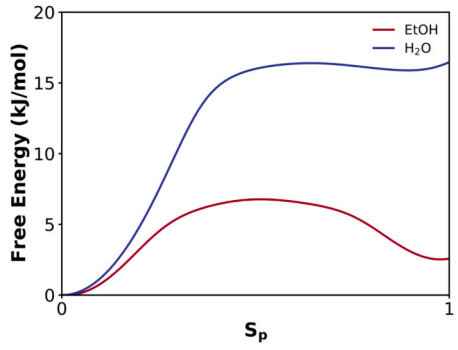

Fig. 3. Free energy profiles for the protonation equilibrium of ethanol and water by the BAS proton plotted along only the protonation state CV, S_p. These profiles show the preference of proton at the BAS in single substrate adsorption.

3.2.2. Protonation of ethanol–water mixtures

To elucidate the nature and protonation thermodynamics of ethanol at the BAS sites in the presence of water we employed WTMetaD for $C_2H_5OH–(H_2O)_n$, $n = 1–4$ (see Section 4.2 of SI for the $n = 4$ case). These simulations used the same two CVs discussed in Section 2.2. The first, S_p, distinguishes the protonation state of ethanol, water and BAS species: $S_p = 0$ when proton resides on BAS oxygens in the zeolite framework, $S_p = 1$ when proton is transferred to ethanol, and $S_p = 3$ when water is protonated. S_d quantifies the distances between the proton carrier and the BAS site.

3.2.2.1. System I: $C_2H_5OH–(H_2O)$. In this competitive case of ethanol and one water molecule, i.e., $C_2H_5OH–(H_2O)$, our WTMetaD simulations show the proton predominantly localizes on ethanol (Fig. 4a-I). This preference is attributed to the greater stability of one protonated ethanol compared to protonated water molecule, also established above in thermodynamics analysis of protonation cases of individual water and ethanol at BAS.

Because of the similar modes of interaction between ethanol and water with the zeolite BAS proton, this suggests that co-adsorbed ethanol and water molecules can form a protonated cluster, similar to the protonated complex formed by two water molecules at the BAS site. To gain detailed structural insight into such mixed protonated cluster of ethanol and water, we employed FESTA code for the extraction of structures corresponding to FES minimum from WTMetaD simulations.

The extracted structures at the FES minima in Fig. 4a-I reveal crucial structural characteristics: In minimum A (see Fig. 4b, Structure IA), the proton resides on ethanol, yielding protonated ethanol that interacts with water through hydrogen bonding while maintaining contact with the BAS site oxygens. This arrangement closely parallels the equilibrium AIMD structure shown in Fig. S3i-a in SI, where protonated ethanol is stabilized by hydrogen bonds to both water and the BAS.

In minimum B (Fig. 4b, Structure IB), the excess proton is taken by water, while it forms hydrogen bond with ethanol and BAS oxygens. In some configurations within this basin, the proton appears partially shared between ethanol and water while water and ethanol are hydrogen-bonded to BAS oxygen giving rise to Zundel-like arrangement. The average O···O distance between ethanol and water is 2.5 Å, supporting the interpretation of a shared proton which is stabilized by cooperative hydrogen bonding between BAS, ethanol and water molecules. These structural observations underscore the complexity of proton localization in mixed solvent-zeolite systems and highlight the significance of both thermodynamic stability and hydrogen-bond network geometry in governing proton dynamics at the molecular scale. They also align with AIMD results (shown in Section 2 in the SI), which show protonated ethanol as the dominant species but allow for interconversion with protonated water through dynamic hydrogen-bond networks.

3.2.2.2. System II: C_2H_5OH-$(H_2O)_2$. At two water loading level, C_2H_5OH-$(H_2O)_2$, the excess proton shows a slight preference for water over ethanol. However, interestingly the FES shows two distinct metastable minima in the region associated with ethanol protonation at $S_p = 1$ (Fig. 4a-II). We hypothesized that these two regions arise from structurally different hydrogen bonded configurations of protonated ethanol. To investigate this, we collected configurations from the WTMetaD enhanced sampled trajectory specifically at $S_p = 1$, which corresponds to ethanol protonation. We then employed SOAP descriptors to characterize the local atomic environments of ethanol and water oxygens as

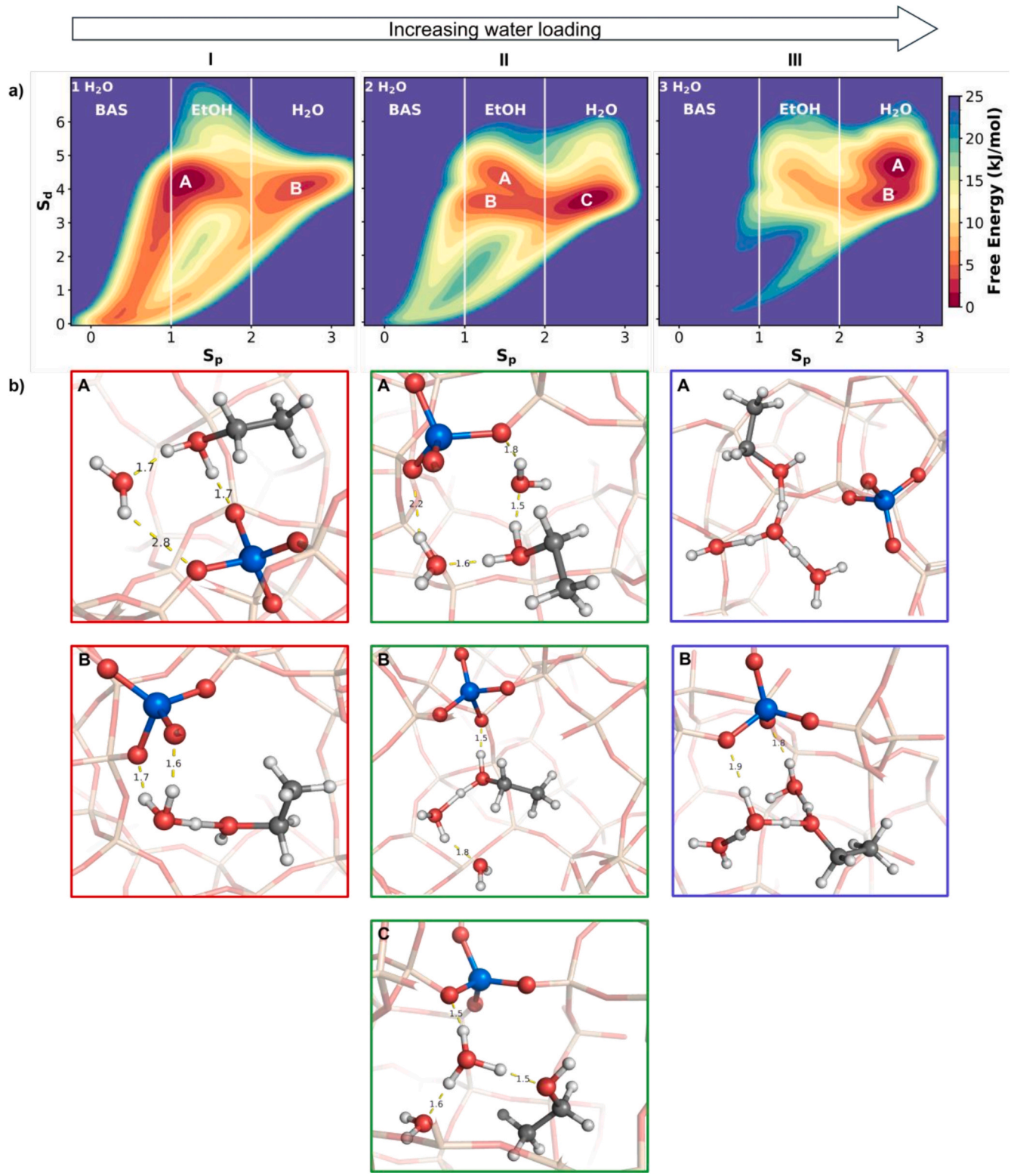

Fig. 4. a) Free energy surfaces for the protonation equilibrium of ethanol by BAS proton with increasing hydration level calculated from statistical reweighting of the simulations two collective variables: S_p, representing the proton location, and S_d, representing the distance of the proton carrier from the BAS site. b) Representative molecular structures (selected from a collection of snapshots corresponding to the free energy minima) are extracted by FESTA method combined with SOAP descriptors. All bond lengths shown are in Å. Atom color coding: aluminum (blue), oxygen (red), hydrogen (white), carbon (grey). For clarity, the silicon and oxygen atoms of the zeolite framework are shown in a transparent representation. (For interpretation of the references to colour in this figure legend, the reader is referred to the web version of this article.)

well as the BAS site. To reduce the dimensionality of the descriptors we applied kernel Principal Component Analysis (kPCA) [112]. For the selected centers, a cut-off of 3.7 was used, with n_{max} and l_{max} values set to 12, 12 respectively. By projecting the first two kPCA eigenvectors of the $S_p = 1$ structures against the collective variable S_d (which measures the distance of protonated ethanol from the BAS), we observed two well-separated structural clusters as shown in Fig. 6. These clusters represent two distinct metastable states of protonated ethanol, differing in the way the protonated ethanol forms hydrogen bonds with the BAS and surrounding water molecules.

In minimum A (Fig. 4b, Structure IIA), ethanol is protonated and hydrogen-bonded to two water molecules, forming a $CH_3OH_2^+$ Eigen-like species. At the same time, the water molecules are hydrogen-bonded to BAS oxygens, resulting in a multifaceted hydrogen-bonding network. In contrast, minimum B (see Fig. 4b, Structure IIB) features protonated ethanol forming a hydrogen-bonded complex with only one water molecule and the BAS.

Finally, the stable minimum corresponding to water protonation ($S_p = 3$) involves structures where the protonated water forms hydrogen bonds with a neighboring water molecule, ethanol, and the BAS. This arrangement produces a characteristic Eigen-type H_3O^+ cluster (see Fig. 4b, Structure IIC).

3.2.2.3. System III: C_2H_5OH–$(H_2O)_3$. Finally, upon increasing the water loading to three molecules C_2H_5OH–$(H_2O)_3$ the protonation equilibrium shifts entirely toward water as depicted in the free energy profiles in Fig. 5. No metastable states corresponding to protonated ethanol are observed in the FES (Fig. 4a-II) at this level of hydration. This result indicates that, within the zeolite confinement, a minimum of three water molecules is sufficient to fully stabilize the excess proton in water, forming hydronium ion clusters. Consequently, the competition between ethanol and water for the proton becomes unidirectional, with water dominating. These water clusters likely act as dynamic catalytic centers, where the hydronium ion plays a central role in mediating reactions involving alcohol and water.

Interestingly, the FES at this hydration level exhibits two distinct minima associated with water protonation, mirroring the dual minima previously observed for ethanol protonation at two-water loading. To probe the molecular origin of these two states, we employed FESTA [111] to extract representative configurations for each minimum. Structural analysis revealed that the two minima differ in the specific interaction between the protonated water cluster and the surrounding ethanol molecule, consistent with AIMD simulation results shown in

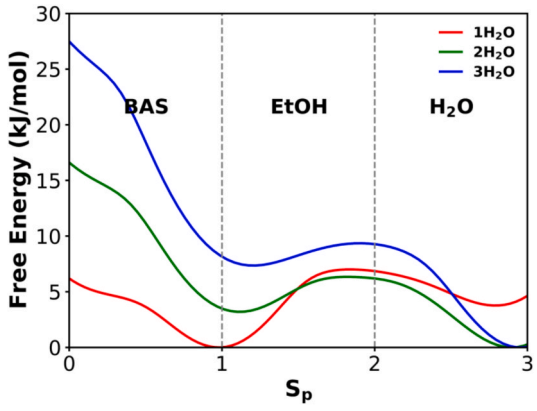

Fig. 5. Free energy profiles for the protonation equilibrium of ethanol with increasing water loading. The profiles were obtained through statistical reweighting of WTMetaD simulations along the collective variable S_p, which characterizes the location of the excess proton. These profiles illustrate the shifting protonation preference from ethanol to water as a function of hydration level.

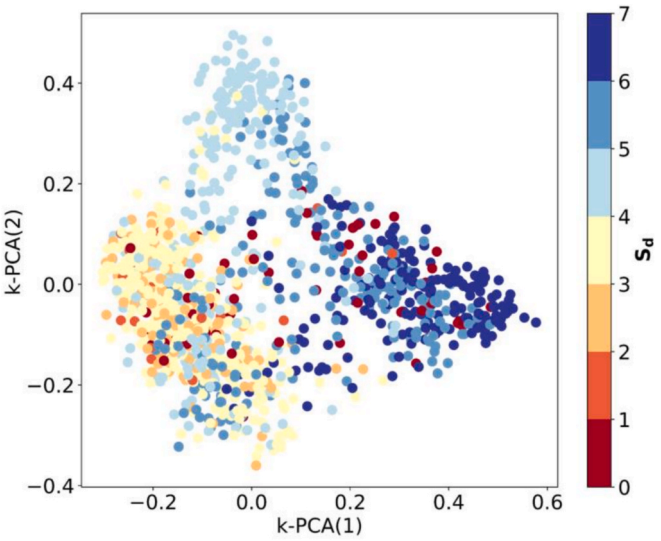

Fig. 6. Projection of the kernel Principal Component Analysis (kPCA) eigenvectors for structures corresponding to ethanol protonation in (C_2H_5OH–$(H_2O)_2$). The projections are plotted against the distance between the protonated ethanol and BAS. This analysis highlights the presence of distinct structural clusters underlying the two metastable states observed in the FES for ethanol protonation.

Fig. S1 of SI. In the dominant configuration of basin **A** (see Fig. 4b, Structure IIIA), the protonated water forms an Eigen-like structure, where the hydronium ion (H_3O^+) is solvated by two water molecules and one ethanol molecule, creating a cluster analogous to H_3O^+·$(H_2O)_3$.

In contrast, minimum **B** exhibits greater configurational diversity. However, the most representative configuration shown in Fig. 4b, Structure IIIB features protonated water hydrogen-bonded to one water molecule, ethanol, and the BAS. Either the water or ethanol is further hydrogen-bonded to another water molecule, which in turn connects to the BAS. Other observed motifs include hydronium bound to one water and one ethanol or solvated by two water molecules alone. Despite these variations, all identified motifs fall within the Eigen-type classification of hydrated proton clusters, which is consistent with the known preference for Eigen-like configurations in both gas-phase, protonated water clusters and bulk aqueous environments. These results indicate that ethanol, under these hydration conditions, can participate in hydrogen bonding with the hydronium ion in a manner similar to water. In C_2H_5OH–$(H_2O)_3$, the system approaches bulk-like hydration behavior [47,49,52], wherein water effectively sequesters the excess proton to form stable hydronium ion clusters, with ethanol serving as an additional solvating partner rather than a proton acceptor. To confirm this trend, we extended our analysis to four water molecules, C_2H_5OH–$(H_2O)_4$ (see FES in Fig. S8 of SI). The results of WTMetaD simulations for this loading of water are fully consistent with C_2H_5OH–$(H_2O)_3$ case, showing only the evidence of water protonation. This confirms that beyond three water molecules, the protonation equilibrium is shifted entirely toward water, with ethanol contributing solely as a secondary solvation partner. Together, these findings support the conclusion that a minimum of three water molecules is sufficient to achieve complete protolysis of water and full stabilization of the excess proton within the zeolite confinement. In all systems including, the baseline (ethanol-only or water-only) systems and the mixed ethanol–water simulations, we observed proton shuttling events involving the BAS, water, and ethanol molecules. In the pure systems, the proton intermittently transfers between the BAS and the adsorbate. In the mixed systems, particularly at higher hydration levels (≥2 H_2O per ethanol), the proton becomes increasingly delocalized across the hydrogen-bonded network. This leads to frequent shuttling between water and ethanol molecules.

This study sheds light on the correlations between the nature of

zeolite/water/alcohol interfaces and catalytic activity, providing thermodynamic and structural insights into the amphiphilic interactions that govern reactivity in confined microporous environments. The delocalization of protons at BAS to in water clusters is not only a fundamental acid–base phenomenon but also directly influences catalytic reactivity. Proton mobility and the formation of extended hydronium–solvent clusters alter the accessibility and lifetime of reactive intermediates, which are central to alcohol dehydration and related transformations. By elucidating the conditions necessary for their formation, this study lays the foundation for quantitatively linking solvation structure to catalytic function under realistic, solvent-rich conditions. Previous kinetic studies in both gas and aqueous phases have shown that water, even as a co-solvent, can either inhibit or promote reactivity depending on its interaction with the solvated proton and the transition state structure. Here, we combine state-of-the-art enhanced-sampling simulations with machine-learning and data-analysis tools to investigate the activated free-energy landscape of proton transfer in alcohol–water–zeolite systems at molecular detail. Our approach enables a quantitative characterization of the energetic and structural requirements for proton transfer including the identification of a critical hydration number of three water molecules and reveals the role of ethanol as a base under confinement, a phenomenon that has not been systematically explored using free-energy calculations.

Our work establishes a direct connection between proton localization, solvation structure, and the dynamic identity of the active species as hydration increases in the presence of ethanol. Whereas previous studies have typically focused on adsorption [113,114], diffusion [115–118], or static energetics of protonated clusters, we provide a unified, dynamical picture linking the evolving solvation environment to catalytically relevant proton-transfer events. These findings establish a foundation for extending solvent-mediated proton transfer concepts to a broader range of alcohols and zeolite frameworks, offering insights into acid catalysis under realistic aqueous–organic conditions and enabling predictive understanding of reactivity in other biomass-derived alcohol systems.

4. Conclusion

In this work, we provide a molecular-level understanding of the mechanism, energetics and thermodynamics of protonation equilibria in ethanol–water mixtures confined within the pores of H-ZSM-5 zeolite. Studies of the local ground state structures based on a global optimization method show that in minimally hydrated systems the BAS generally retains the proton, although several low-lying alternative configurations (within 20 kJ/mol) exist where ethanol/water moiety is protonated. With increasing hydration, the proton is progressively stabilized away from the BAS, but the BAS still plays a role in stabilizing the solvated proton/ethanol/water moieties. In general, based on the ground state energetics, protonation of ethanol is becoming accessible even at the $1H_2O$ hydration state through proton equilibrium. Inclusion of thermal effects in enhanced molecular dynamics simulations is marked by frequent proton exchange between BAS, ethanol, and water. Ethanol protonation becoming dominant at one-water loading highlights the critical contribution of entropy and collective hydrogen-bond dynamics. WTMetaD using MLP provides a comprehensive free energy perspective. Compared with the limiting cases of only ethanol or water, where the proton is firmly bound to the BAS, mixed ethanol–water systems show competitive protonation. In the presence of one water molecule, ethanol acts as the stronger base; however, upon adsorption of two or more water molecules, the equilibrium shifts toward protonation of water clusters, which increasingly exhibit bulk-like solvation behavior. Equilibrium AIMD trajectories benchmark the trained MLP demonstrating that this method can effectively capture the nuanced interactions of water–ethanol clusters at a fraction of the computational cost whilst significantly improving the sampling and having a significant impact on the relative free energetics. Using machine learning with generalized chemical environment descriptors, we characterize the structures of the main free energy basin. The analysis identifies key structural fingerprints of metastable protonated states, highlighting complex hydrogen-bonded networks of BAS, ethanol, and water, where ethanol directly contributes to the formation of Eigen-like structures.

In summary, this study highlights the protonation behavior of alcohol–water mixtures in the confined environment of acidic zeolite nanopores. These findings are highly relevant for understanding the initial steps of alcohol reactivity at zeolite–water interfaces, which play a crucial role in many catalytic processes of industrial and environmental importance. Although the global optimization process is only considering the energy surface, it still captures the additional pertinent structures, determined as higher-lying minima. Using a global optimization approach of low computational cost, we can obtain a quick overview of the relevant structures that dominate chemical reactivity, which is naturally addressed by the appropriate collective variables used with the WTMetaD approach.

CRediT authorship contribution statement

Princy Jarngal: Writing – review & editing, Writing – original draft, Visualization, Validation, Software, Methodology, Formal analysis, Data curation, Conceptualization. **Benjamin A. Jackson:** Writing – review & editing, Writing – original draft, Visualization, Validation, Methodology, Formal analysis, Data curation, Conceptualization. **Simuck F. Yuk:** Writing – review & editing, Writing – original draft, Visualization, Validation, Supervision, Methodology, Formal analysis, Data curation, Conceptualization. **Difan Zhang:** Writing – review & editing, Writing – original draft, Visualization, Validation, Supervision, Methodology, Formal analysis, Data curation, Conceptualization. **Mal-Soon Lee:** Writing – review & editing, Writing – original draft, Visualization, Validation, Supervision, Formal analysis, Data curation, Conceptualization. **Maria Cristina Menziani:** Writing – review & editing, Writing – original draft, Visualization, Validation, Methodology, Formal analysis, Data curation, Conceptualization. **Vassiliki-Alexandra Glezakou:** Writing – review & editing, Writing – original draft, Visualization, Validation, Supervision, Software, Resources, Project administration, Methodology, Investigation, Funding acquisition, Formal analysis, Data curation, Conceptualization. **Roger Rousseau:** Writing – review & editing, Writing – original draft, Visualization, Validation, Supervision, Software, Resources, Project administration, Methodology, Investigation, Funding acquisition, Formal analysis, Data curation, Conceptualization. **GiovanniMaria Piccini:** Writing – review & editing, Writing – original draft, Visualization, Validation, Supervision, Software, Resources, Project administration, Methodology, Investigation, Funding acquisition, Formal analysis, Data curation, Conceptualization.

Declaration of competing interest

The authors declare that they have no known competing financial interests or personal relationships that could have appeared to influence the work reported in this paper.

Acknowledgements

P.J and G.P. gratefully acknowledge the grant funded by the Deutsche Forschungsgemeinschaft (DFG, German Research Foundation) under Germany's Excellence Strategy, Cluster of Excellence 2186 "The Fuel Science Center" ID 390919832. They also acknowledge computing time provided to them at the NHR Center NHR4CES at RWTH Aachen University (project ID p0024037). This is funded by the Federal Ministry of Research, Technology and Space, and the state governments participating on the basis of the resolutions of the GWK for national high performance computing at universities. B.A.J. and M.-S.L. were supported by the U.S. Department of Energy (DOE), Office of Science, Office of Basic Energy Sciences (BES), Division of Chemical Sciences, and

Geosciences & Biosciences at Pacific Northwest National Laboratory (PNNL) (FWP 47319). PNNL is a multiprogram national laboratory operated for DOE by Battelle under Contract DE-AC05-76RL01830. D.Z., V.-A.G., and R.R. acknowledge the support from the U.S. Department of Energy, Office of Science, Office of Basic Energy Sciences, Chemical Sciences, Geosciences, and Biosciences Division, Catalysis Science Program (Grant ERKCC96) at Oak Ridge National Laboratory (ORNL). ORNL is operated by UT-Battelle under contract no. DE-AC05-00OR22725 for the U.S. Department of Energy. This research partly used resources of the National Energy Research Scientific Computing Center (NERSC), a Department of Energy User Facility using NERSC award BES-ERCAP0032412 and BES-ERCAP0032671. The views expressed herein are those of the authors and do not reflect the position of the United States Military Academy, the Department of the Army, the Department of Defense, or the U.S. Government.

Appendix A. Supplementary data

Supplementary data to this article can be found online at https://doi.org/10.1016/j.jcat.2025.116658.

Data availability

Data will be made available on request.

References

[1] W.O. Haag, R.M. Lago, P.B. Weisz, The active site of acidic aluminosilicate catalysts, Nature 309 (5969) (1984) 589–591, https://doi.org/10.1038/309589a0.
[2] G. Busca, Acid catalysts in industrial hydrocarbon chemistry, Chem. Rev. 107 (11) (2007) 5366–5410, https://doi.org/10.1021/cr068042e.
[3] W. Vermeiren, J.-P. Gilson, Impact of zeolites on the petroleum and petrochemical industry, Top. Catal. 52 (9) (2009) 1131–1161, https://doi.org/10.1007/s11244-009-9271-8.
[4] A. Primo, H. Garcia, Zeolites as catalysts in oil refining, Chem. Soc. Rev. 43 (22) (2014) 7548–7561, https://doi.org/10.1039/C3CS60394F.
[5] P. del Campo, C. Martínez, A. Corma, Activation and conversion of alkanes in the confined space of zeolite-type materials, Chem. Soc. Rev. 50 (15) (2021) 8511–8595, https://doi.org/10.1039/D0CS01459A.
[6] A. Corma, Inorganic solid acids and their use in acid-catalyzed hydrocarbon reactions, Chem. Rev. 95 (3) (1995) 559–614, https://doi.org/10.1021/cr00035a006.
[7] A. Corma, H. Garcia, S. Iborra, J. Primo, Modified faujasite zeolites as catalysts in organic reactions: esterification of carboxylic acids in the presence of HY zeolites, J. Catal. 120 (1) (1989) 78–87, https://doi.org/10.1016/0021-9517(89)90252-2.
[8] Ó. de la Iglesia, R. Mallada, M. Menéndez, J. Coronas, Continuous zeolite membrane reactor for esterification of ethanol and acetic acid, Chem. Eng. J. 131 (1) (2007) 35–39, https://doi.org/10.1016/j.cej.2006.12.015.
[9] K.A. Tarach, J. Tekla, W. Makowski, U. Filek, K. Mlekodaj, V. Girman, M. Choi, K. Góra-Marek, Catalytic dehydration of ethanol over hierarchical ZSM-5 zeolites: studies of their acidity and porosity properties, Catal. Sci. Technol. 6 (10) (2016) 3568–3584, https://doi.org/10.1039/C5CY01866H.
[10] E. Dumitriu, V. Hulea, I. Fechete, A. Auroux, J.-F. Lacaze, C. Guimon, The aldol condensation of lower aldehydes over MFI zeolites with different acidic properties, Microporous Mesoporous Mater. 43 (3) (2001) 341–359, https://doi.org/10.1016/S1387-1811(01)00265-7.
[11] Solvent-determined mechanistic pathways in zeolite-H-BEA-catalysed phenol alkylation | Nature Catalysis. https://www.nature.com/articles/s41929-017-0015-z (accessed 2025-09-29).
[12] T.N. Pham, T. Sooknoi, S.P. Crossley, D.E. Resasco, Ketonization of carboxylic acids: mechanisms, catalysts, and implications for biomass conversion, ACS Catal. 3 (11) (2013) 2456–2473, https://doi.org/10.1021/cs400501h.
[13] S. Mardiana, N.J. Azhari, T. Ilmi, G.T.M. Kadja, Hierarchical zeolite for biomass conversion to biofuel: a review, Fuel 309 (2022) 122119, https://doi.org/10.1016/j.fuel.2021.122119.
[14] C. Bornes, I.C.M.S. Santos-Vieira, R. Vieira, L. Mafra, M.M.Q. Simões, J. Rocha, Challenges and opportunities for zeolites in biomass upgrading: impediments and future directions, Catal. Today 419 (2023) 114159, https://doi.org/10.1016/j.cattod.2023.114159.
[15] T. Ennaert, J.V. Aelst, J. Dijkmans, R.D. Clercq, W. Schutyser, M. Dusselier, D. Verboekend, B.F. Sels, Potential and challenges of zeolite chemistry in the catalytic conversion of biomass, Chem. Soc. Rev. 45 (3) (2016) 584–611, https://doi.org/10.1039/C5CS00859J.
[16] M.J. Climent, A. Corma, S. Iborra, Conversion of biomass platform molecules into fuel additives and liquid hydrocarbon fuels, Green Chem. 16 (2) (2014) 516–547, https://doi.org/10.1039/C3GC41492B.
[17] E. Taarning, C.M. Osmundsen, X. Yang, B. Voss, S.I. Andersen, C.H. Christensen, Zeolite-catalyzed biomass conversion to fuels and chemicals, Energy Environ. Sci. 4 (3) (2011) 793–804, https://doi.org/10.1039/C004518G.
[18] A. Vjunov, J.L. Fulton, T. Huthwelker, S. Pin, D. Mei, G.K. Schenter, N. Govind, D. M. Camaioni, J.Z. Hu, J.A. Lercher, Quantitatively probing the Al distribution in zeolites, J. Am. Chem. Soc. 136 (23) (2014) 8296–8306, https://doi.org/10.1021/ja501361v.
[19] A. Vjunov, J.L. Fulton, D.M. Camaioni, J.Z. Hu, S.D. Burton, I. Arslan, J. A. Lercher, Impact of aqueous medium on zeolite framework integrity, Chem. Mater. 27 (9) (2015) 3533–3545, https://doi.org/10.1021/acs.chemmater.5b01238.
[20] L. Smith, A.K. Cheetham, R.E. Morris, L. Marchese, J.M. Thomas, P.A. Wright, J. Chen, On the nature of water bound to a solid acid catalyst, Science 271 (5250) (1996) 799–802, https://doi.org/10.1126/science.271.5250.799.
[21] V. Termath, F. Haase, J. Sauer, J. Hutter, M. Parrinello, Understanding the nature of water bound to solid acid surfaces. *Ab initio* simulation on HSAPO-34, J. Am. Chem. Soc. 120 (33) (1998) 8512–8516, https://doi.org/10.1021/ja981549p.
[22] J. Limtrakul, P. Chuichay, S. Nokbin, Effect of high coverages on proton transfer in the zeolite/water system, J. Mol. Struct. 560 (1) (2001) 169–177, https://doi.org/10.1016/S0022-2860(00)00737-7.
[23] C. Pazé, S. Bordiga, C. Lamberti, M. Salvalaggio, A. Zecchina, G. Bellussi, Acidic properties of H−β zeolite as probed by bases with proton affinity in the 118−204 Kcal Mol-1 range: a FTIR investigation, J. Phys. Chem. B 101 (24) (1997) 4740–4751, https://doi.org/10.1021/jp970649z.
[24] S. Bordiga, C. Lamberti, F. Bonino, A. Travert, F. Thibault-Starzyk, Probing zeolites by vibrational spectroscopies, Chem. Soc. Rev. 44 (20) (2015) 7262–7341, https://doi.org/10.1039/C5CS00396B.
[25] A. Zecchina, F. Geobaldo, G. Spoto, S. Bordiga, G. Ricchiardi, R. Buzzoni, G. Petrini, FTIR investigation of the formation of neutral and ionic hydrogen-bonded complexes by interaction of H-ZSM-5 and H-mordenite with CH3CN and H2O: comparison with the H-NAFION superacidic system, J. Phys. Chem. 100 (41) (1996) 16584–16599, https://doi.org/10.1021/jp960433h.
[26] F. Wakabayashi, J.N. Kondo, K. Domen, C. Hirose, FT-IR study of H218O adsorption on H-ZSM-5: direct evidence for the hydrogen-bonded adsorption of water, J. Phys. Chem. 100 (5) (1996) 1442–1444, https://doi.org/10.1021/jp953089h.
[27] Q. Liu, J.A. van Bokhoven, Water structures on acidic zeolites and their roles in catalysis, Chem. Soc. Rev. 53 (6) (2024) 3065–3095, https://doi.org/10.1039/D3CS00404J.
[28] N.S. Gould, S. Li, H.J. Cho, H. Landfield, S. Caratzoulas, D. Vlachos, P. Bai, B. Xu, Understanding solvent effects on adsorption and protonation in porous catalysts, Nat. Commun. 11 (1) (2020) 1060, https://doi.org/10.1038/s41467-020-14860-6.
[29] N. Pfriem, P.H. Hintermeier, S. Eckstein, S. Kim, Q. Liu, H. Shi, L. Milakovic, Y. Liu, G.L. Haller, E. Baráth, Y. Liu, J.A. Lercher, Role of the ionic environment in enhancing the activity of reacting molecules in zeolite pores, Science 372 (6545) (2021) 952–957, https://doi.org/10.1126/science.abh3418.
[30] L.R. MacGillivray, J.L. Atwood, A chiral spherical molecular assembly held together by 60 hydrogen bonds, Nature 389 (6650) (1997) 469–472, https://doi.org/10.1038/38985.
[31] R. Capelli, G. Piccini, Atomistic insights into hydrogen-bonded supramolecular capsule self-assembly dynamics, J. Phys. Chem. C 128 (1) (2024) 635–641, https://doi.org/10.1021/acs.jpcc.3c07148.
[32] W. Zhang, G. Cheng, G.L. Haller, Y. Liu, J.A. Lercher, Rate enhancement of acid-catalyzed alcohol dehydration by supramolecular organic capsules, ACS Catal. 10 (22) (2020) 13371–13376, https://doi.org/10.1021/acscatal.0c03625.
[33] T.-R. Li, G. Piccini, K. Tiefenbacher, Supramolecular capsule-catalyzed highly β-selective furanosylation independent of the SN1/SN2 reaction pathway, J. Am. Chem. Soc. 145 (7) (2023) 4294–4303, https://doi.org/10.1021/jacs.2c13641.
[34] T.-R. Li, F. Huck, G. Piccini, K. Tiefenbacher, Mimicry of the proton wire mechanism of enzymes inside a supramolecular capsule enables β-selective O-glycosylations, Nat. Chem. 14 (9) (2022) 985–994, https://doi.org/10.1038/s41557-022-00981-6.
[35] T.-R. Li, C. Das, G. Piccini, K. Tiefenbacher, Tetrafluororesorcin[4]Arene hexameric capsule enables the expansion of the reactivity space in supramolecular catalysis, J. Am. Chem. Soc. 147 (13) (2025) 11108–11116, https://doi.org/10.1021/jacs.4c17029.
[36] D.E. Resasco, S.P. Crossley, B. Wang, J.L. White, Interaction of Water with zeolites: a review, Catal. Rev. 63 (2) (2021) 302–362, https://doi.org/10.1080/01614940.2021.1948301.
[37] M. Krossner, J. Sauer, Interaction of water with brønsted acidic sites of zeolite catalysts. *Ab initio* study of 1:1 and 2:1 surface complexes, J. Phys. Chem. 100 (15) (1996) 6199–6211, https://doi.org/10.1021/jp952775d.
[38] S.A. Zygmunt, L.A. Curtiss, L.E. Iton, M.K. Erhardt, Computational studies of water adsorption in the zeolite H-ZSM-5, J. Phys. Chem. 100 (16) (1996) 6663–6671, https://doi.org/10.1021/jp952913z.
[39] J.A. Pople, J.S. Binkley, R. Seeger, Theoretical models incorporating electron correlation, Int. J. Quantum Chem 10 (S10) (1976) 1–19, https://doi.org/10.1002/qua.560100802.
[40] D.H. Olson, S.A. Zygmunt, M.K. Erhardt, L.A. Curtiss, L.E. Iton, Evidence for dimeric and tetrameric water clusters in HZSM-5, Zeolites 18 (5) (1997) 347–349, https://doi.org/10.1016/S0144-2449(97)00024-9.
[41] H. Jobic, A. Tuel, M. Krossner, J. Sauer, Water in interaction with acid sites in H-ZSM-5 zeolite does not form hydroxonium ions. A comparison between neutron scattering results and *Ab initio* calculations, J. Phys. Chem. 100 (50) (1996) 19545–19550, https://doi.org/10.1021/jp9619954.

[42] G. Piccini, M. Alessio, J. Sauer, *Ab initio* study of methanol and ethanol adsorption on brønsted sites in zeolite H-MFI, Phys. Chem. Chem. Phys. 20 (30) (2018) 19964–19970, https://doi.org/10.1039/C8CP03632B.

[43] K. Alexopoulos, M.-S. Lee, Y. Liu, Y. Zhi, Y. Liu, M.-F. Reyniers, G.B. Marin, V.-A. Glezakou, R. Rousseau, J.A. Lercher, Anharmonicity and confinement in zeolites: structure, spectroscopy, and adsorption free energy of ethanol in H-ZSM-5, J. Phys. Chem. C 120 (13) (2016) 7172–7182, https://doi.org/10.1021/acs.jpcc.6b00923.

[44] Y. Jeanvoine, J.G. Ángyán, G. Kresse, J. Hafner, On the nature of water interacting with brønsted acidic sites. *Ab initio* molecular dynamics study of hydrated HSAPO-34, J. Phys. Chem. B 102 (38) (1998) 7307–7310, https://doi.org/10.1021/jp981667z.

[45] K. Stanciakova, J.N. Louwen, B.M. Weckhuysen, R.E. Bulo, F. Göltl, Understanding water–zeolite interactions: on the accuracy of density functionals, J. Phys. Chem. C 125 (37) (2021) 20261–20274, https://doi.org/10.1021/acs.jpcc.1c04270.

[46] A. Vjunov, M. Wang, N. Govind, T. Huthwelker, H. Shi, D. Mei, J.L. Fulton, J. A. Lercher, Tracking the chemical transformations at the brønsted acid site upon water-induced deprotonation in a zeolite pore, Chem. Mater. 29 (21) (2017) 9030–9042, https://doi.org/10.1021/acs.chemmater.7b02133.

[47] J.H. Hack, X. Ma, Y. Chen, J.P. Dombrowski, N.H.C. Lewis, C. Li, H.H. Kung, G. A. Voth, A. Tokmakoff, Proton dissociation and delocalization under stepwise hydration of zeolite HZSM-5, J. Phys. Chem. C 127 (32) (2023) 16175–16186, https://doi.org/10.1021/acs.jpcc.3c03611.

[48] V. Vener, X. Rozanska, J. Sauer, Protonation of water clusters in the cavities of acidic zeolites: (H 2 O) n ·H-chabazite, n = 1–4, Phys. Chem. Chem. Phys. 11 (11) (2009) 1702–1712, https://doi.org/10.1039/B817905K.

[49] E. Grifoni, G. Piccini, J.A. Lercher, V.-A. Glezakou, R. Rousseau, M. Parrinello, Confinement effects and acid strength in zeolites, Nat. Commun. 12 (1) (2021) 2630, https://doi.org/10.1038/s41467-021-22936-0.

[50] P. Liu, D. Mei, Identifying free energy landscapes of proton-transfer processes between brønsted acid sites and water clusters inside the zeolite pores, J. Phys. Chem. C 124 (41) (2020) 22568–22576, https://doi.org/10.1021/acs.jpcc.0c07033.

[51] S.A. Zygmunt, L.A. Curtiss, L.E. Iton, Protonation of an H_2O dimer by a zeolitic Brønsted acid site, J. Phys. Chem. B 105 (15) (2001) 3034–3038, https://doi.org/10.1021/jp003469p.

[52] M.V. Vener, X. Rozanska, J. Sauer, Protonation of water clusters in the cavities of acidic zeolites: (H2O)n·H-chabazite, n = 1–4, Phys. Chem. Chem. Phys. 11 (11) (2009) 1702–1712, https://doi.org/10.1039/B817905K.

[53] P.W. Kletnieks, J.O. Ehresmann, J.B. Nicholas, J.F. Haw, Adsorbate clustering and proton transfer in zeolites: NMR spectroscopy and theory, ChemPhysChem 7 (1) (2006) 114–116, https://doi.org/10.1002/cphc.200500313.

[54] H.-P. Cheng, Water clusters: fascinating hydrogen-bonding networks, solvation shell structures, and proton motion, J. Phys. Chem. A 102 (31) (1998) 6201–6204, https://doi.org/10.1021/jp981433f.

[55] Y. Kawai, S. Yamaguchi, Y. Okada, K. Takeuchi, Y. Yamauchi, S. Ozawa, H. Nakai, Reactions of protonated water clusters H+(H2O)n (n=1–6) with dimethylsulfoxide in a guided ion beam apparatus, Chem. Phys. Lett. 377 (1) (2003) 69–73, https://doi.org/10.1016/S0009-2614(03)01095-9.

[56] M. Wang, N.R. Jaegers, M.-S. Lee, C. Wan, J.Z. Hu, H. Shi, D. Mei, S.D. Burton, D. M. Camaioni, O.Y. Gutiérrez, V.-A. Glezakou, R. Rousseau, Y. Wang, J.A. Lercher, Genesis and stability of hydronium ions in zeolite channels, J. Am. Chem. Soc. 141 (8) (2019) 3444–3455, https://doi.org/10.1021/jacs.8b07969.

[57] F. Haase, J. Sauer, 1H NMR chemical shifts of ammonia, methanol, and water molecules interacting with broensted acid sites of zeolite catalysts: Ab-initio calculations, J. Phys. Chem. 98 (12) (1994) 3083–3085, https://doi.org/10.1021/j100063a006.

[58] A. Laio, M. Parrinello, Escaping free-energy minima, Proc. Natl. Acad. Sci. 99 (20) (2002) 12562–12566, https://doi.org/10.1073/pnas.202427399.

[59] A. Barducci, G. Bussi, M. Parrinello, Well-tempered metadynamics: a smoothly converging and tunable free-energy method, Phys. Rev. Lett. 100 (2) (2008) 020603, https://doi.org/10.1103/PhysRevLett.100.020603.

[60] E. Grifoni, G. Piccini, M. Parrinello, Microscopic description of acid–base equilibrium, Proc. Natl. Acad. Sci. 116 (10) (2019) 4054–4057, https://doi.org/10.1073/pnas.1819771116.

[61] E. Grifoni, G. Piccini, M. Parrinello, Tautomeric equilibrium in condensed phases, J. Chem. Theory Comput. 16 (10) (2020) 6027–6031, https://doi.org/10.1021/acs.jctc.0c00519.

[62] G. Li, B. Wang, D.E. Resasco, Water-mediated heterogeneously catalyzed reactions, ACS Catal. 10 (2) (2020) 1294–1309, https://doi.org/10.1021/acscatal.9b04637.

[63] Y. Liu, A. Vjunov, H. Shi, S. Eckstein, D.M. Camaioni, D. Mei, E. Baráth, J. A. Lercher, Enhancing the catalytic activity of hydronium ions through constrained environments, Nat. Commun. 8 (1) (2017) 14113, https://doi.org/10.1038/ncomms14113.

[64] A. Vjunov, M.Y. Hu, J. Feng, D.M. Camaioni, D. Mei, J.Z. Hu, C. Zhao, J. A. Lercher, Following solid-acid-catalyzed reactions by MAS NMR spectroscopy in liquid phase—zeolite-catalyzed conversion of cyclohexanol in water, Angew. Chem. Int. Ed. 53 (2) (2014) 479–482, https://doi.org/10.1002/anie.201306673.

[65] H. Shi, S. Eckstein, A. Vjunov, D.M. Camaioni, J.A. Lercher, Tailoring nanoscopic confines to maximize catalytic activity of hydronium ions, Nat. Commun. 8 (1) (2017) 15442, https://doi.org/10.1038/ncomms15442.

[66] D. Mei, J.A. Lercher, Effects of local water concentrations on cyclohexanol dehydration in H-BEA zeolites, J. Phys. Chem. C 123 (41) (2019) 25255–25266, https://doi.org/10.1021/acs.jpcc.9b07738.

[67] P. Liu, W. Hao, D. Mei, Understanding the effects of water molecules on cyclohexanol dehydration over zeolitic acid sites, J. Phys. Chem. C 125 (28) (2021) 15283–15291, https://doi.org/10.1021/acs.jpcc.1c03846.

[68] A.C. Fogarty, F.-X. Coudert, A. Boutin, D. Laage, Reorientational dynamics of water confined in zeolites, ChemPhysChem 15 (3) (2014) 521–529, https://doi.org/10.1002/cphc.201300928.

[69] T. Zhou, P. Bai, J.I. Siepmann, A.E. Clark, Deconstructing the confinement effect upon the organization and dynamics of water in hydrophobic nanoporous materials: lessons learned from zeolites, J. Phys. Chem. C 121 (40) (2017) 22015–22024, https://doi.org/10.1021/acs.jpcc.7b04991.

[70] D.T. Bregante, M.C. Chan, J.Z. Tan, E.Z. Ayla, C.P. Nicholas, D. Shukla, D. W. Flaherty, The shape of water in zeolites and its impact on epoxidation catalysis, Nat. Catal. 4 (9) (2021) 797–808, https://doi.org/10.1038/s41929-021-00672-4.

[71] H.K. Chau, H.D. Mai, A. Gumidyala, T.N. Pham, D.-P. Bui, A.D. D'Amico, I. Alalq, D.T. Glatzhofer, J.L. White, S.P. Crossley, Effect of water on cumene dealkylation over H-ZSM-5 zeolites, ACS Catal. 13 (13) (2023) 9158–9170, https://doi.org/10.1021/acscatal.2c05759.

[72] R. Gounder, A.J. Jones, R.T. Carr, E. Iglesia, Solvation and acid strength effects on catalysis by faujasite zeolites, J. Catal. 286 (2012) 214–223, https://doi.org/10.1016/j.jcat.2011.11.002.

[73] R. Gounder, M.E. Davis, Beyond shape selective catalysis with zeolites: hydrophobic void spaces in zeolites enable catalysis in liquid water, AIChE J 59 (9) (2013) 3349–3358, https://doi.org/10.1002/aic.14016.

[74] J.S. Bates, B.C. Bukowski, J. Greeley, R. Gounder, Structure and solvation of confined water and water–ethanol clusters within microporous brønsted acids and their effects on ethanol dehydration catalysis, Chem. Sci. 11 (27) (2020) 7102–7122, https://doi.org/10.1039/D0SC02589E.

[75] D. Mei, J.A. Lercher, Mechanistic insights into aqueous phase propanol dehydration in H-ZSM-5 Zeolite, AIChE J 63 (1) (2017) 172–184, https://doi.org/10.1002/aic.15517.

[76] Y. Zhi, H. Shi, L. Mu, Y. Liu, D. Mei, D.M. Camaioni, J.A. Lercher, Dehydration pathways of 1-propanol on HZSM-5 in the presence and absence of water, J. Am. Chem. Soc. 137 (50) (2015) 15781–15794, https://doi.org/10.1021/jacs.5b09107.

[77] K. Chen, J. Damron, C. Pearson, D. Resasco, L. Zhang, J.L. White, Zeolite catalysis: water can dramatically increase or suppress alkane C–H bond activation, ACS Catal. 4 (9) (2014) 3039–3044, https://doi.org/10.1021/cs500858d.

[78] M.A. Mellmer, C. Sener, J.M.R. Gallo, J.S. Luterbacher, D.M. Alonso, J. A. Dumesic, Solvent effects in acid-catalyzed biomass conversion reactions, Angew. Chem. Int. Ed. 53 (44) (2014) 11872–11875, https://doi.org/10.1002/anie.201408359.

[79] M.A. Mellmer, C. Sanpitakseree, B. Demir, P. Bai, K. Ma, M. Neurock, J. A. Dumesic, Solvent-enabled control of reactivity for liquid-phase reactions of biomass-derived compounds, Nat. Catal. 1 (3) (2018) 199–207, https://doi.org/10.1038/s41929-018-0027-3.

[80] S. Kim, M.-S. Lee, D.M. Camaioni, O.Y. Gutiérrez, V.-A. Glezakou, N. Govind, T. Huthwelker, R. Zhao, R. Rousseau, J.L. Fulton, J.A. Lercher, Self-organization of 1-propanol at H-ZSM-5 Brønsted acid sites, JACS Au 3 (9) (2023) 2487–2497, https://doi.org/10.1021/jacsau.3c00259.

[81] I. Batatia, D.P. Kovacs, G. Simm, C. Ortner, G. Csanyi, MACE: higher order equivariant message passing neural networks for fast and accurate force fields, Adv. Neural Inf. Process. Syst. 35 (2022) 11423–11436.

[82] G. Wang, C. Wang, X. Zhang, Z. Li, J. Zhou, Z. Sun, Machine learning interatomic potential: bridge the gap between small-scale models and realistic device-scale simulations, iScience 27 (5) (2024) 109673, https://doi.org/10.1016/j.isci.2024.109673.

[83] J. Falk, L. Bonati, P. Novelli, M. Parrinello, M. Pontil, Transfer learning for atomistic simulations using GNNs and Kernel mean embeddings, arXiv January 21, (2024), Doi: 10.48550/arXiv.2306.01589.

[84] A. Erlebach, M. Šípka, I. Saha, P. Nachtigall, C.J. Heard, L. Grajciar, A reactive neural network framework for water-loaded acidic zeolites, Nat. Commun. 15 (1) (2024) 4215, https://doi.org/10.1038/s41467-024-48609-2.

[85] A. Omranpour, J. Elsner, K.N. Lausch, J. Behler, Machine learning potentials for heterogeneous catalysis, ACS Catal. 15 (3) (2025) 1616–1634, https://doi.org/10.1021/acscatal.4c06717.

[86] D. Zhang, M.Z. Makoś, R. Rousseau, V.-A. Glezakou, RANGE: a robust adaptive nature-inspired global explorer of potential energy surfaces, J. Chem. Phys. 163 (15) (2025) 152501, https://doi.org/10.1063/5.0288910.

[87] A.K. Rappe, C.J. Casewit, K.S. Colwell, W.A.I. Goddard, W.M. Skiff, UFF, a full periodic table force field for molecular mechanics and molecular dynamics simulations, J. Am. Chem. Soc. 114 (25) (1992) 10024–10035, https://doi.org/10.1021/ja00051a040.

[88] I. Batatia, P. Benner, Y. Chiang, A.M. Elena, D.P. Kovács, J. Riebesell, X.R. Advincula, M. Asta, M. Avaylon, W.J. Baldwin, F. Berger, N. Bernstein, A. Bhowmik, F. Bigi, S.M. Blau, V. Cărare, M. Ceriotti, S. Chong, J.P. Darby, S. De F. D. Pia, V.L. Deringer, R. Elijošius, Z. El-Machachi, F. Falcioni, E. Fako, A.C. Ferrari, J.L.A. Gardner, M.J. Gawkowski, A. Genreith-Schriever, J. George, R.E.A. Goodall, J. Grandel, C.P. Grey, P. Grigorev, S. Han, W. Handley, H.H. Heenen, K. Hermansson, C. Holm, C.H. Ho, S. Hofmann, J. Jaafar, K.S. Jakob, H. Jung, V. Kapil, A.D. Kaplan, N. Karimitari, J.R. Kermode, P. Kourtis, N. Kroupa, J. Kullgren, M.C. Kuner, D. Kuryla, G. Liepuoniute, C. Lin, J.T. Margraf, I.-B. Magdău, A. Michaelides, J.H. Moore, A.A. Naik, S.P. Niblett, S.W. Norwood, N. O'Neill, C. Ortner, K.A. Persson, K. Reuter, A.S. Rosen, L.A.M. Rosset, L.L. Schaaf, C. Schran, B.X. Shi, E. Sivonxay, T.K. Stenczel, V. Svahn, C. Sutton, T.D.

Swinburne, J. Tilly, C. van Oord der, S. Vargas, E. Varga-Umbrich, T. Vegge, M. Vondrák, Y. Wang, W.C. Witt, T. Wolf, F. Zills, G. Csányi, A foundation model for atomistic materials chemistry, arXiv September 4, (2025). Doi: 10.48550/arXiv.2401.00096.

[89] P. Willett, The calculation of molecular structural similarity: principles and practice, Mol. Inform. 33 (6–7) (2014) 403–413, https://doi.org/10.1002/minf.201400024.

[90] S.A. Bero, A.K. Muda, Y.H. Choo, N.A. Muda, S.F. Pratama, Similarity measure for molecular structure: a brief review, J. Phys. Conf. Ser. 892 (1) (2017) 012015, https://doi.org/10.1088/1742-6596/892/1/012015.

[91] G. Collinge, S.F. Yuk, M.-T. Nguyen, M.-S. Lee, V.-A. Glezakou, R. Rousseau, Effect of collective dynamics and anharmonicity on entropy in heterogenous catalysis: building the case for advanced molecular simulations, ACS Catal. 10 (16) (2020) 9236–9260, https://doi.org/10.1021/acscatal.0c01501.

[92] G.M. Torrie, J.P. Valleau, Nonphysical sampling distributions in monte carlo free-energy estimation: umbrella sampling, J. Comput. Phys. 23 (2) (1977) 187–199, https://doi.org/10.1016/0021-9991(77)90121-8.

[93] D. Mendels, G. Piccini, M. Parrinello, Collective variables from local fluctuations, J. Phys. Chem. Lett. 9 (11) (2018) 2776–2781, https://doi.org/10.1021/acs.jpclett.8b00733.

[94] G. Piccini, D. Mendels, M. Parrinello, Metadynamics with discriminants: a tool for understanding chemistry, J. Chem. Theory Comput. 14 (10) (2018) 5040–5044, https://doi.org/10.1021/acs.jctc.8b00634.

[95] J.P. Perdew, K. Burke, M. Ernzerhof, Generalized gradient approximation made simple, Phys. Rev. Lett. 77 (18) (1996) 3865–3868, https://doi.org/10.1103/PhysRevLett.77.3865.

[96] S. Grimme, Semiempirical GGA-type density functional constructed with a long-range dispersion correction, J. Comput. Chem. 27 (15) (2006) 1787–1799, https://doi.org/10.1002/jcc.20495.

[97] J. VandeVondele, J. Hutter, Gaussian basis sets for accurate calculations on molecular systems in gas and condensed phases, J. Chem. Phys. 127 (11) (2007) 114105, https://doi.org/10.1063/1.2770708.

[98] S. Goedecker, M. Teter, J. Hutter, Separable dual-space Gaussian pseudopotentials, Phys. Rev. B 54 (3) (1996) 1703–1710, https://doi.org/10.1103/PhysRevB.54.1703.

[99] C. Hartwigsen, S. Goedecker, J. Hutter, Relativistic separable dual-space gaussian pseudopotentials from H to Rn, Phys. Rev. B 58 (7) (1998) 3641–3662, https://doi.org/10.1103/PhysRevB.58.3641.

[100] M. Krack, Pseudopotentials for H to Kr optimized for gradient-corrected exchange-correlation functionals, Theor. Chem. Acc. 114 (1) (2005) 145–152, https://doi.org/10.1007/s00214-005-0655-y.

[101] T.D. Kühne, M. Iannuzzi, M. Del Ben, V.V. Rybkin, P. Seewald, F. Stein, T. Laino, R.Z. Khaliullin, O. Schütt, F. Schiffmann, D. Golze, J. Wilhelm, S. Chulkov, M. H. Bani-Hashemian, V. Weber, U. Borštnik, M. Taillefumier, A.S. Jakobovits, A. Lazzaro, H. Pabst, T. Müller, R. Schade, M. Guidon, S. Andermatt, N. Holmberg, G.K. Schenter, A. Hehn, A. Bussy, F. Belleflamme, G. Tabacchi, A. Glöß, M. Lass, I. Bethune, C.J. Mundy, C. Plessl, M. Watkins, J. VandeVondele, M. Krack, J. Hutter, CP2K: an electronic structure and molecular dynamics software package - quickstep: efficient and accurate electronic structure calculations, J. Chem. Phys. 152 (19) (2020) 194103, https://doi.org/10.1063/5.0007045.

[102] G.A. Tribello, M. Bonomi, D. Branduardi, C. Camilloni, G. Bussi, PLUMED 2: new feathers for an old bird, Comput. Phys. Commun. 185 (2) (2014) 604–613, https://doi.org/10.1016/j.cpc.2013.09.018.

[103] J.P. Darby, J.R. Kermode, G. Csányi, Compressing local atomic neighbourhood descriptors, NPJ Comput. Mater. 8 (1) (2022) 166, https://doi.org/10.1038/s41524-022-00847-y.

[104] H. Zhang, V. Juraskova, F. Duarte, Modelling chemical processes in explicit solvents with machine learning potentials, Nat. Commun. 15 (1) (2024) 6114, https://doi.org/10.1038/s41467-024-50418-6.

[105] L. Himanen, M.O.J. Jäger, E.V. Morooka, F. Federici Canova, Y.S. Ranawat, D. Z. Gao, P. Rinke, A.S. Foster, DScribe: library of descriptors for machine learning in materials science, Comput. Phys. Commun. 247 (2020) 106949, https://doi.org/10.1016/j.cpc.2019.106949.

[106] S. Grimme, J. Antony, S. Ehrlich, H. Krieg, A consistent and accurate *Ab initio* parametrization of density functional dispersion correction (DFT-D) for the 94 elements H-Pu, J. Chem. Phys. 132 (15) (2010) 154104, https://doi.org/10.1063/1.3382344.

[107] S. Grimme, S. Ehrlich, L. Goerigk, Effect of the damping function in dispersion corrected density functional theory, J. Comput. Chem. 32 (7) (2011) 1456–1465, https://doi.org/10.1002/jcc.21759.

[108] C. Schran, K. Brezina, O. Marsalek, Committee neural network potentials control generalization errors and enable active learning, J. Chem. Phys. 153 (10) (2020) 104105, https://doi.org/10.1063/5.0016004.

[109] A.P. Thompson, H.M. Aktulga, R. Berger, D.S. Bolintineanu, W.M. Brown, P. S. Crozier, P.J. In 't Veld, A. Kohlmeyer, S.G. Moore, T.D. Nguyen, R. Shan, M. J. Stevens, J. Tranchida, C. Trott, S.J. Plimpton, LAMMPS - a flexible simulation tool for particle-based materials modeling at the atomic, meso, and continuum scales, Comput. Phys. Commun. 271 (2022) 108171, https://doi.org/10.1016/j.cpc.2021.108171.

[110] H. Windeck, F. Berger, J. Sauer, Chemically accurate predictions for water adsorption on brønsted sites of zeolite H-MFI, Phys. Chem. Chem. Phys. 26 (36) (2024) 23588–23599, https://doi.org/10.1039/D4CP02851A.

[111] V. Istomin, G. Piccini, FESTA: a polygon-based approach for extracting relevant structures from free energy surfaces obtained in molecular simulations, J. Chem. Inf. Model. 65 (1) (2025) 1–6, https://doi.org/10.1021/acs.jcim.4c01022.

[112] H. Hoffmann, Kernel PCA for novelty detection, Pattern Recognit. 40 (3) (2007) 863–874, https://doi.org/10.1016/j.patcog.2006.07.009.

[113] S. Pahari, M. Dorneles de Mello, M.S. Shah, T.R. Josephson, L. Ren, H.G. T. Nguyen, R.D. Van Zee, M. Tsapatsis, J.I. Siepmann, Ethanol and water adsorption in conventional and hierarchical all-silica MFI zeolites, ACS Phys. Chem. Au 2 (2) (2022) 79–88, https://doi.org/10.1021/acsphyschemau.1c00026.

[114] K. Zhang, R.P. Lively, J.D. Noel, M.E. Dose, B.A. McCool, R.R. Chance, W.J. Koros, Adsorption of water and ethanol in MFI-type zeolites, Langmuir 28 (23) (2012) 8664–8673, https://doi.org/10.1021/la301122h.

[115] R. Krishna, J.M. van Baten, Highlighting pitfalls in the Maxwell–Stefan modeling of water–alcohol mixture permeation across pervaporation membranes, J. Membr. Sci. 360 (1) (2010) 476–482, https://doi.org/10.1016/j.memsci.2010.05.049.

[116] C. Zhang, X. Yang, Molecular dynamics simulation of ethanol/water mixtures for structure and diffusion properties, Fluid Phase Equilib. 231 (1) (2005) 1–10, https://doi.org/10.1016/j.fluid.2005.03.018.

[117] Z. Keyvanloo, A. Nakhaei Pour, F. Moosavi, S.M. Kamali Shahri, Molecular dynamic simulation studies of adsorption and diffusion behaviors of methanol and ethanol through ZSM-5 zeolite, J. Mol. Graph. Model. 110 (2022) 108048, https://doi.org/10.1016/j.jmgm.2021.108048.

[118] J.Y. Wu, Q.L. Liu, Y. Xiong, A.M. Zhu, Y. Chen, Molecular simulation of water/alcohol mixtures' adsorption and diffusion in zeolite 4A membranes, J. Phys. Chem. B 113 (13) (2009) 4267–4274, https://doi.org/10.1021/jp805923k.